

Quantum Hamiltonian Algorithms for Maximum Independent Sets

Xianjue Zhao(赵贤觉),¹ Peiyun Ge(葛培云),² Hongye Yu(余泓烨),³
Li You(尤力),^{2, 4, 5} Frank Wilczek,^{6, 7, 8, 9} and Biao Wu(吴飙)^{1, 10, 11, *}

¹ International Center for Quantum Materials, School of Physics, Peking University, Beijing 100871, China

² State Key Laboratory of Low Dimensional Quantum Physics,

Department of Physics, Tsinghua University, Beijing 100084, China

³ Department of Physics and Astronomy, Stony Brook University, Stony Brook, NY 11794, USA

⁴ Frontier Science Center for Quantum Information, Beijing, China

⁵ Beijing Academy of Quantum Information Sciences, Beijing 100193, China

⁶ Center for Theoretical Physics, MIT, Cambridge, Massachusetts 02139, USA

⁷ T. D. Lee Institute and Wilczek Quantum Center,

Shanghai Jiao Tong University, Shanghai 200240, China

⁸ Department of Physics, Stockholm University, Stockholm SE-106 91, Sweden

⁹ Department of Physics, Arizona State University, Tempe, Arizona 85287, USA

¹⁰ Wilczek Quantum Center, University of Science and Technology of China, Shanghai 201315, China

¹¹ Hefei National Laboratory, Hefei 230088, China

(Dated: July 10, 2024)

We compare two quantum Hamiltonian algorithms that address the maximum independent set problem: one based on emergent non-abelian gauge matrix in adiabatic evolution of an energetically isolated manifold of states; and one based on designed application of single-qubit operations. We demonstrate that they are *mathematically* equivalent, though at first sight they appear quite different. Despite their mathematical equivalence, their most straightforward physical implementations are different. Our numerical simulations show significant differences in performance, and suggest improved experimental protocols. Intriguingly, this equivalence unveils a deeper connection. We also demonstrate that the PXP model, recently prominent in quantum dynamics research, arises as the non-abelian gauge matrix governing quantum diffusion over the median graph of all independent sets.

Introduction - Identifying large independent sets within a graph provides a well-defined and readily simulated domain with different complexity classes, including NP-hard. As such, this makes it an attractive test-bed for new algorithms and techniques. In particular, it is interesting to ask whether quantum algorithms might offer advantages over classical algorithms for these problems.

Recently two apparently different quantum algorithms have been proposed for the problem of maximum independent set (MIS). In a graph, an independent set is a collection of vertices, none of which are directly connected by edges. Among all the independent sets, the ones with the largest number of vertices are called maximum independent sets (see Fig. 1 for an example). Finding a MIS is NP-hard on classical computers [1]. Approximating MIS also poses a significant challenge for classical computer [2–5].

One quantum algorithm, which we shall call the PK algorithm, was introduced and refined in Refs.[6, 7]. It leverages a general approach that utilizes emergent non-abelian gauge potentials arising during adiabatic state evolution to achieve the desired interactions. The other [8], which we shall call the HV algorithm, is based on carefully designed application of one-body operators. Interestingly, we demonstrate in this work that these seemingly distinct approaches are mathematically equivalent.

Specifically, the Hamiltonian used in the PK algorithm can be understood as the HV Hamiltonian transformed into the interaction picture.

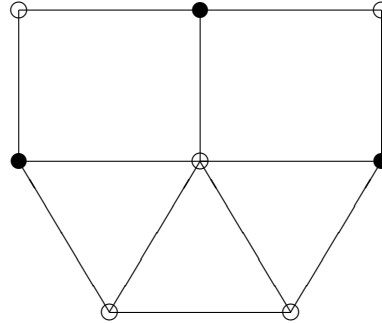


FIG. 1: A graph. The solid circles form one of its maximum independent sets.

Despite their mathematical equivalence, these two algorithms offer distinct perspectives that yield valuable insights. We discover both novel experimental protocols and deeper theoretical understanding. When implemented straightforwardly on Rydberg atom arrays without optimization, our numerical simulations suggest that the PK algorithm's adiabatic path performs significantly better. This suggests that we can optimize the performance of future large tweezer arrays [9], and move close to the goal of demonstrating quantum advantage in a

* wubiao@pku.edu.cn

natural problem.

The equivalence also reveals a fascinating connection. The PXP model [10], known for its quantum many-body scarring phenomenon and experimentally realized with Rydberg atom arrays [11], is essentially the non-abelian gauge matrix in the PK algorithm. This relationship holds significant promise. From one perspective, the PXP model, traditionally viewed as a many-body problem, can now be seen as single-particle quantum diffusion over a median graph [12–14]. This median graph's vertices represent the independent sets of the original graph. In another perspective, the PXP model, originally defined on a special one-dimensional graph, can be extended to other graphs. This extension could enrich the exploration of quantum many-body scarring and other quantum dynamical phenomena.

Quantum algorithms - In this work, we compare two quantum algorithms: one was proposed theoretically in [6, 7] and the other was realized in a recent experiment [8]. We will refer to the former as PK algorithm and the latter as HV algorithm. We find that there two algorithms are mathematically equivalent. Specifically, the Hamiltonian in the PK algorithm can be viewed as the HV Hamiltonian in the interaction picture. Nevertheless, these two quantum algorithms offer distinctive perspectives on the same problem.

The HV algorithm for MIS in a recent experiment [8] uses the following Hamiltonian

$$\hat{H}_L = \frac{\hbar}{2} \sum_{j=1}^n [\Omega(t) e^{i\varphi(t)} |0\rangle_j \langle 1|_j + \text{h.c.} - 2\Delta(t) \hat{n}_j + \sum_{i < j} V_{ij} \hat{n}_i \hat{n}_j], \quad (1)$$

where $|0\rangle_j$ represents that the atom at site j not in the excited Rydberg state, while $|1\rangle_j$ represents that it is excited. For a graph with n vertices of single atoms, the operator $\hat{n}_j = |1\rangle_j \langle 1|_j$ denotes the Rydberg state fraction operator for site j . The term V_{ij} describes the interaction strength between two excited Rydberg atoms situated at sites i and j . A repulsive interaction V_{ij} imposes an energy penalty on multi-atom configurations in which both i and $j \neq i$ are excited. Such interactions correspond, in the graph problem, to the existence of a line connecting the sites. $\Omega(t), \varphi(t), \Delta(t)$ are control functions whose implementation defines the algorithm. In general, the goal of MIS algorithms of the type discussed here is to evolve into configuration with many disconnected excited states. These correspond to low-energy states at late times, when $\Omega \rightarrow 0$ and Δ approaches a positive constant.

With the pseudo-spin operators $\sigma_j^z = 2\hat{n}_j - 1$, $\sigma_j^+ = |1\rangle_j \langle 0|_j$, and $\sigma_j^- = |0\rangle_j \langle 1|_j$ we can rewrite the Hamiltonian H_L (up to an irrelevant time-dependent c-number) as

$$\hat{H}_L = \hat{H}_1(t) + \hat{H}_2, \quad (2)$$

where

$$\begin{aligned} \hat{H}_1(t) &= \frac{\hbar}{2} \Omega(t) \cos \varphi(t) \sum_j \sigma_j^x + \frac{\hbar}{2} \Omega(t) \sin \varphi(t) \sum_j \sigma_j^y \\ &\quad - \frac{\hbar}{2} \Delta(t) \sum_j \sigma_j^z, \end{aligned} \quad (3)$$

and

$$\hat{H}_2 = \sum_{i < j} \frac{V_{ij}}{4} (1 + \sigma_i^z)(1 + \sigma_j^z). \quad (4)$$

Here \hat{H}_L is partitioned into two parts: $\hat{H}_1(t)$, a single-spin Hamiltonian which depends on time, and \hat{H}_2 , the interactions between spins which is time-independent.

The PK algorithm in Refs [6, 7] proposed theoretically a seemingly different Hamiltonian for the MIS problem. The Hamiltonian is

$$\hat{H}_A(t) = U(t) \hat{H}_0 U^\dagger(t), \quad (5)$$

where

$$\hat{H}_0 = \frac{V_0}{4} \sum_{i < j} (1 + \sigma_i^z)(1 + \sigma_j^z) = V_0 \sum_{i < j} \hat{n}_i \hat{n}_j, \quad (6)$$

and $U(t) = V(t)^{\otimes n}$ with $V(t)$ being a unitary matrix for spin-1/2. When $V(t)$ changes adiabatically as specified in the references, one can find the MISs as the ground states according to the PK algorithm.

Equivalence - We will demonstrate in the following that the Hamiltonians \hat{H}_L and \hat{H}_A are theoretically equivalent. The starting point is to note that \hat{H}_0 and \hat{H}_2 are essentially the same for $V_{ij} > 0$, or repulsive interaction between Rydberg atoms. This is because one can always choose a $V_0 > 0$ such that all $V_{ij} > V_0$. In this case, \hat{H}_0 and \hat{H}_2 have the same set of ground states, which correspond to all independent sets of a given graph. Therefore, only \hat{H}_2 will be referenced to in the following discussion.

Consider a Hamiltonian system $\hat{H}_S(t) = \hat{H}_1(t) + \hat{H}_2$, which is similar to \hat{H}_L . The evolution of its wave function $|\Phi_S(t)\rangle$ is described by the Schrödinger equation

$$i \frac{d}{dt} |\Phi_S(t)\rangle = [\hat{H}_1(t) + \hat{H}_2] |\Phi_S(t)\rangle. \quad (7)$$

We can go to the interaction picture with the following unitary evolution operator

$$U_I(t) = \mathcal{T} e^{-i \int_0^t \hat{H}_1(t') dt'}, \quad (8)$$

and the quantum state $|\Phi_I(t)\rangle$ in the interaction picture is related to the state in the Schrödinger picture as follows

$$|\Phi_I(t)\rangle = U_I^\dagger(t) |\Phi_S(t)\rangle, \quad (9)$$

which satisfies the following equation

$$i \frac{d}{dt} |\Phi_I(t)\rangle = U_I^\dagger(t) \hat{H}_2 U_I(t) |\Phi_I(t)\rangle. \quad (10)$$

When $U_I(t) = U^\dagger(t)$, it is clear that the state $|\Phi_I(t)\rangle$ will follow the evolution governed by the Hamiltonian $\hat{H}_A(t)$ as specified in Eq. (5). With the form of $U(t)$ given in Refs. [6, 7], the condition $U_I(t) = U^\dagger(t)$ allows us to deduce $\hat{H}_1(t)$. If $\hat{H}_1(t)$ takes the same form of $\hat{H}_1(t)$ in Eq. (3), the Hamiltonian $\hat{H}_A(t)$ is equivalent to $\hat{H}_L(t)$.

After some calculations, we obtain

$$\begin{aligned}\hat{H}_1 &= -iU^\dagger(t)\partial_t U(t), \\ &= (\vec{n} \times \vec{n}') \cdot \sum_j \vec{\sigma}_j.\end{aligned}\quad (11)$$

where $\vec{n}'(t) = d\vec{n}(t)/dt$ and

$$\vec{n}(t) = \left(\sin \frac{\theta}{2} \cos \phi, \sin \frac{\theta}{2} \sin \phi, \cos \frac{\theta}{2}\right), \quad (12)$$

with θ and ϕ changing with time according to $\theta = \omega_\theta t$, $\phi = \omega_\phi t$. The physical meaning of θ, ϕ can be found in [6, 7].

The $\hat{H}_1(t)$ in Eq. (11) is of the same form of $\hat{H}_1(t)$ in Eq. (3). We thus have shown that the Hamiltonian $\hat{H}_A(t)$ is equivalent to $\hat{H}_L(t)$.

In the experiment [8], the quantum state is in the Schrödinger picture, which as we show above is related to the state in the interaction picture according to Eq. (9). At the end $t = T$ of the adiabatic evolution specified in Ref. [7], we have $\theta = \pi$ and $\phi = 0$. This means that

$$U_I^\dagger(T) = U(T) = [\vec{n}(T) \cdot \vec{\sigma}]^{\otimes n} = [\sigma_x]^{\otimes n}. \quad (13)$$

Its action is to flip every qubit. For the PK algorithm as discussed in Ref. [7], one needs to flip all the spins to get the right answer for the MIS. So the two flips cancel out and we can adopt $|\Phi_S(t)\rangle$ obtained in the experiment as the final result.

Non-abelian gauge potential and PXP model - We note that $-\hat{H}_1(t)$ is actually a non-abelian gauge potential. To see this, if we choose $U'(t) = U(t)\Lambda^\dagger(t)$, where $\Lambda(t)$ is unitary, we will find

$$\begin{aligned}-\hat{H}'_1 &= i\Lambda U^\dagger \partial_t (U\Lambda^\dagger), \\ &= \Lambda(-\hat{H}_1)\Lambda^\dagger + i\Lambda\partial_t\Lambda^\dagger,\end{aligned}\quad (14)$$

which is precisely the gauge transformation of a non-abelian gauge potential. Furthermore, if we project $-\hat{H}_1$ onto the subspace of the ground states of \hat{H}_2 (or the independent sets of the corresponding graph), we will obtain the non-abelian gauge matrix A of the PK algorithm, namely

$$-A(t) = P\hat{H}_1(t)P, \quad (15)$$

where P is the projection onto the ground states of \hat{H}_2 . If $V_{ij} \gg \|\hat{H}_1(t)\|$, Eq. (15) gives an effective Hamiltonian on the subspace of \hat{H}_2 up to first-order. This shows that the Hamiltonian system governed by the gauge matrix A is essentially the PXP model [10], which is known for

its quantum many-body scarring phenomenon and has been experimentally realized with Rydberg atom arrays [11]. The specific correspondence between them is rather straightforward. For the original PXP model in which $\Omega(t) = \Omega, \Delta(t) = 0, \varphi(t) = 0$, we only need to set $\theta(t) = \pi/2, \phi(t) = \Omega t$ in the PK algorithm. Quenching the PXP model as a method to find the maximum independent set has also been proposed recently[15], but still requires exponentially long runtime due to the many-body scars.

This intriguing relation offers fresh new perspectives on the PXP model, a many-body system originally defined on a one-dimensional chain. We can now view the one-dimensional chain as the underlying graph of the PXP model, with the Néel-type state corresponding to the MIS of this simple graph.

This paves the way for an extension of the PXP model that applies to more complex graphs. For any graph there exists a dual graph, in which each vertex represents an independent set, and each edge connects a pair of independent sets whose Hamming distance is one (see the Appendix for details). This dual graph is a median graph [12–14]. The many-body PXP model, through its relation to A , can be reinterpreted as a single-particle quantum diffusion over the dual graph. This extension has the potential to enrich the study of quantum many-body scarring. (The oscillating behavior for $\theta = \pi/2$ in Fig. 8 of Ref.[6] can be explained in these terms. We will discuss these ideas in more detail elsewhere.)

The relation between A and H_1 in Eq.(15) shows that, when the graph is fixed, the energy gap of A is proportional to $-\hat{H}_1$. This means that to have a successful adiabatic path, it is better to let \hat{H}_1 have an as large energy gap as possible, in particular, in the late stage of the evolution. The adiabatic path in the PK algorithm indeed has this feature. For the PK algorithm, we have $\hat{H}_1 = (\vec{n} \times \vec{n}') \cdot \sum_j \vec{\sigma}_j$. Its energy spectrum is simple and the energy gap is

$$\Delta E = 2|\vec{n} \times \vec{n}'| = \sqrt{4\omega_\phi^2 \sin^2 \frac{\theta}{2} + \omega_\theta^2}. \quad (16)$$

In the algorithm, as θ varies from 0 to π , ΔE is steadily increasing and reaches its maximum at the end of the evolution. This is confirmed by the numerical study which follows.

Numerical Comparison - While the PK algorithm [6, 7] and the HV algorithm [8] are formally equivalent, they are motivated in different ways and offer different perspectives. The HV algorithm can be readily implemented experimentally while the PK algorithm gives an intuitive insight on how the algorithm is capable of finding MIS in an inherently quantum way. Combined we now have a quantum MIS algorithm that is easy to implement experimentally and exhibit potential advantages over its classical counterparts.

The Hamiltonian \hat{H}_2 has many degenerate ground states, which correspond to all the independent sets of a graph, and the minimum gap between them and the excited states is V_0 , the minimum interaction strength

between Rydberg atoms. When the changing rates ω_ϕ and ω_θ are much smaller than V_0/\hbar in the PK algorithm, the system stays and evolves in the sub-Hilbert space of the degenerate ground states of \hat{H}_2 . Its evolution in the sub-Hilbert space is governed by a non-abelian gauge matrix A , which has a minimum energy gap δ . When $\omega_\theta/\omega_\phi \ll \delta$, at the end of evolution $T = \pi/\omega_\theta$, the system displays significant amplitudes to be in states which are either MIS or its good approximations [7]. It is clear from this insight that, for the quantum algorithm to be effective, one requires:

$$V_0/\hbar \gg \omega_\phi \gg \omega_\theta/\delta. \quad (17)$$

The explanation and physical origin of the dimensionless energy gap δ were given in Refs.[6, 7].

The two changing rates ω_ϕ and ω_θ in the PK algorithm [6, 7] are related to the parameters Δ , Ω and φ in the experimental protocol [8] as follows:

$$\Delta(t) = -2\omega_\phi \sin^2 \frac{\omega_\theta t}{2}, \quad (18)$$

$$\varphi(t) = \arctan \frac{\omega_\phi \sin \omega_\theta t \sin \omega_\phi t - \omega_\theta \cos \omega_\phi t}{\omega_\phi \sin \omega_\theta t \cos \omega_\phi t + \omega_\theta \sin \omega_\phi t}, \quad (19)$$

$$\Omega(t) = \sqrt{\omega_\phi^2 \sin^2(\omega_\theta t) + \omega_\theta^2}, \quad (20)$$

This adiabatic path can be simplified further with a single bit unitary matrix $V_s(t) = V(t)U_s(t) = (\vec{n}(t) \cdot \vec{\sigma})U_s(t)$, where

$$U_s = \begin{pmatrix} 1 & 0 \\ 0 & e^{i\phi(t)} \end{pmatrix}. \quad (21)$$

The simplified path is given by

$$\Delta(t) = \omega_\phi \cos(\omega_\theta t), \quad (22)$$

$$\varphi(t) = -\arctan \frac{\omega_\theta}{\omega_\phi \sin(\omega_\theta t)} + \pi, \quad (23)$$

$$\Omega(t) = \sqrt{\omega_\phi^2 \sin^2(\omega_\theta t) + \omega_\theta^2}. \quad (24)$$

This is shown in Fig.2 as dashed lines. Our analysis below finds that this path exhibit several advantages over the ones discussed in Ref.[8].

In Ref.[8], two different variational methods are used to find an optimized evolution path using classical mathematical search over a restricted set of trial paths. One is called the quantum approximate optimization algorithm and the other is called variational quantum adiabatic algorithm. For the quantum approximate optimization algorithm, it appears that the experimental protocol (as described above) does not quite implement the optimized evolution path faithfully, which would require intermittent absence of interaction terms. For the variational quantum adiabatic algorithm, it starts with an unoptimized path as shown Fig.2A and then the path is optimized with the help of a classical computer and experimental inputs.

We have compared the performances of the two paths in Fig.2 with graphs of seven vertices numerically. With

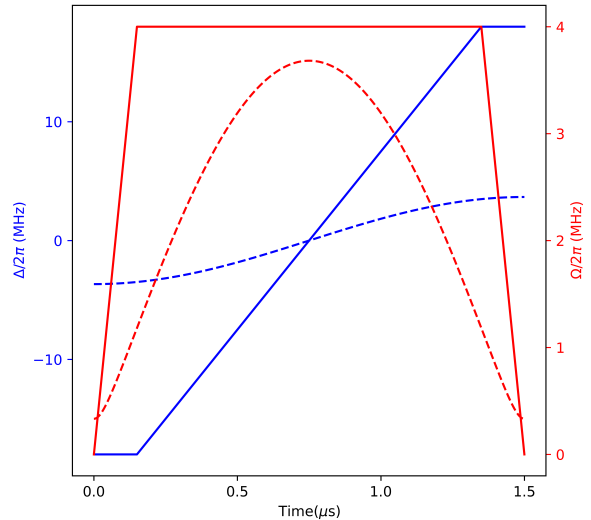


FIG. 2: The unoptimized path of variational quantum adiabatic algorithm is represented by the solid lines, the same as the path given in FIG. S8. of [8]. The adiabatic path of the PK algorithm, given by Eqs. (22, 24), is drawn as the dashed lines with $\omega_\theta = \pi/T$ and $\omega_\phi/\omega_\theta = -11$.

1000 graphs that are randomly generated, the PK algorithm has a minimum success rate of 83.784% and an average success rate of 97.370%. In contrast, the variational quantum adiabatic algorithm has an average success rate of 45.129%. Further numerical results show that in most cases where the variational quantum adiabatic algorithm fails, the algorithms ends in states of non-independent sets, as shown in Fig.3C. We note $\varphi(t) = 0$ is chosen in our numerical calculation. To implement PK algorithm faithfully, one actually needs to change $\varphi(t)$ as Eq. (23). Numerical results show that this does not affect the performance of the PK algorithm. We find that with $\varphi(t)$ following Eq. (23), the PK algorithm has a minimum success rate of 86.247% and an average success rate of 99.122%. Though optimized quantum adiabatic algorithm paths might be more competitive (or even superior), the excellent performance of a bare-bones implementation of PK is noteworthy.

ACKNOWLEDGMENTS

XJZ acknowledges discussions with Fangcheng Wang. XJZ and BW are supported by National Natural Science Foundation of China (Grants No. 92365202 and No. 11921005), and Shanghai Municipal Science and Technology Major Project (Grant No.2019SHZDZX01). PYG and LY are supported by the National Natural Science Foundation of China (NSFC)(Grants No. 12361131576 and No. 92265205), and by the Innovation Program

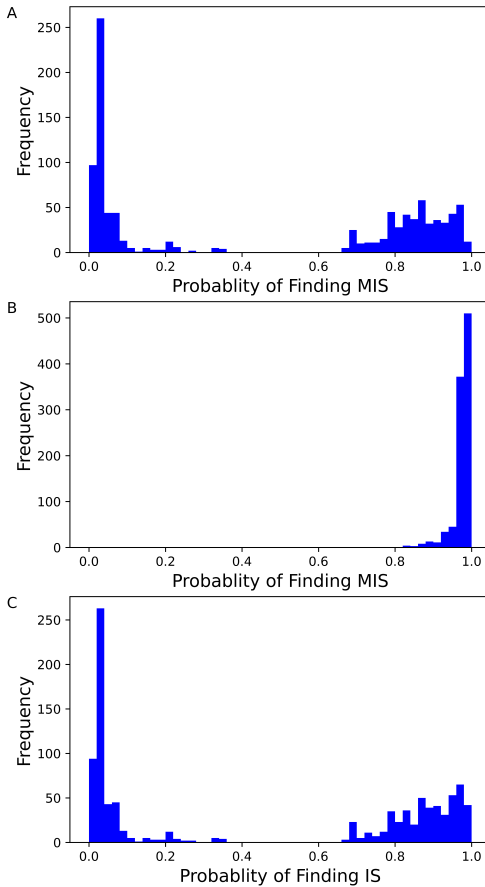


FIG. 3: Performances of the variational quantum adiabatic algorithm and the PK algorithms on 1000 unit disk graphs with 7 vertices. In the numerical simulation, we adopt the experimental parameters [8], that is, $V_{NN}/h = 107$ MHz, $V_{NNN}/h = 13$ MHz, $T = 1.5 \mu\text{s}$. **(A)**.The average success rate using the unoptimized path of variational quantum adiabatic algorithm is 45.129%. **(B)**.The average success rate using the adiabatic path of the PK algorithm is 97.370%. **(C)**.The average rate of ending in states of independent sets using the unoptimized path of variational quantum adiabatic algorithm is 46.132%, which means in most unsuccessful cases, the unoptimized path of variational quantum adiabatic algorithm gives states of non-independent sets.

for Quantum Science and Technology (2021ZD0302100). FW is supported by the U.S. Department of Energy under grant Contract Number DE-SC0012567, by the European Research Council under grant 742104, and by the Swedish Research Council under Contract No. 335-2014-7424.

[1] M. Xiao and H. Nagamochi, *Information and Computation* **255**, 126 (2017).

[2] H. Johan, *Acta Math.* **182**, 105 (1999).

[3] D. Zuckerman, *Proceedings of the Thirty-Eighth Annual ACM Symposium on Theory of Computing* (New York: Association for Computing Machinery) p 681 (2006).

[4] A. Coja-Oghlan and C. Efthymiou, *Random Struct. and Algorithms* **47**, 436 (2015).

[5] A. M. Frieze, *Discrete Math.* **81**, 171 (1990).

[6] Biao Wu, Hongye Yu, Frank Wilczek, “*Quantum independent-set problem and non-Abelian adiabatic mixing*”, *Physical Review A* **101**, 012318 (2020).

[7] Hongye Yu, Frank Wilczek, Biao Wu, “*Quantum Algorithm for Approximating Maximum Independent Sets*”, Chinese Physics Letters **38**, 030304 (2021).

[8] S. Ebadi et al., “*Quantum optimization of maximum independent set using Rydberg atom arrays*”, *Science* **376**, 1209 (2022).

[9] H. J. Manetsch, G. Nomura, E. Bataille, K. H. Leung, X. Lv, and M. Endres, arXiv:2403.12021 (2024).

[10] Turner, C.J., Michailidis, A.A., Abanin, D.A. et al., “*Weak ergodicity breaking from quantum many-body scars*”, *Nature Phys* **14**, 745 (2018).

[11] Bernien, H., Schwartz, S., Keesling, A. et al., “*Probing many-body dynamics on a 51-atom quantum simulator*”, *Nature* **551**, 579 (2017).

[12] T. J. Schaefer, in *Proceedings of the tenth annual ACM symposium on Theory of computing* (ACM, New York,

1978), STOC, pp. 216–226.

[13] H.-J. Bandelt and V. Chepoi, *Contemporary Mathematics* **453**, 49 (2008).

[14] <https://en.wikipedia.org/wiki/2-satisfiability>.

[15] Schiffer, B., Wild, D., Maskara, N., Cain, M., Lukin, M. & Samajdar, R. Circumventing superexponential runtimes for hard instances of quantum adiabatic optimization. *Physical Review Research* **6**, 013271 (2024).

Appendix A: Dual Graph

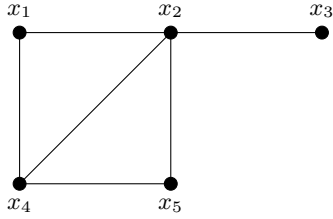


FIG. 4: A graph with 5 vertices and 6 edges.

A dual graph exists for any graph, composed of all its independent sets as the vertices, and connected by edges if and only if the Hamming distance of the corresponding independent sets is one. We use the graph in Fig.4 as an example to illustrate dual graph. We assign each of its vertices a boolean variable. For this example, the five boolean variables are x_1, x_2, x_3, x_4, x_5 . Each of its independent set can then be denoted by a binary

string. For example, $\{0, 0, 0, 0, 0\}$ represents the empty set, $\{0, 1, 0, 0, 0\}$ represents the independent set with only one vertex $\{x_2\}$, $\{1, 0, 1, 0, 1\}$ represents the maximum independent set $\{x_1, x_3, x_5\}$, etc. As each independent set is denoted by a binary string, we can define the Hamming distance between them as the Hamming distance between the corresponding binary strings. For example, the Hamming distance between the empty set and the set with one vertex $\{x_2\}$ is one. The Hamming distance between the empty set and the MIS $\{x_1, x_3, x_5\}$ is three.

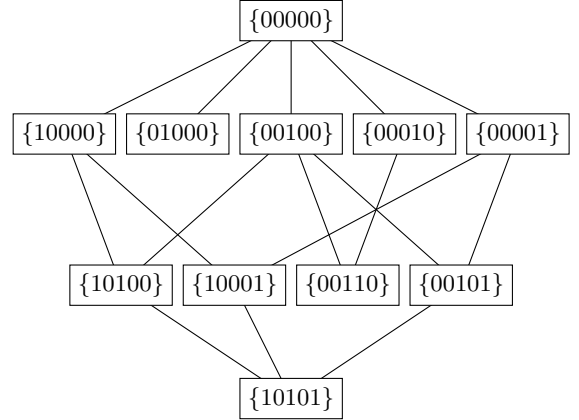


FIG. 5: The dual graph of the graph in Fig.4. Each box (or vertex) represents an independent set.

The graph of Fig.4 has 11 independent sets, that are shown in Fig.5 as marked boxes, or vertices of the dual graph that are connected by an edge between a pair of vertices if their Hamming distance is one. For any graph, its dual graph is a median graph.